Journal of Manufacturing Processes 72 (2021) 61–70

Contents lists available at ScienceDirect

Journal of Manufacturing Processes

journal homepage: www.elsevier.com/locate/manpro

Formation of leaf-shaped microstructure on Zr-based metallic glass via nanosecond pulsed laser irradiation

Yongfeng Qian [a], Hu Huang [a,*], Chao Wang [a], Peng Yu [b], Jinkai Xu [b], Zhiyu Zhang [c]

[a] Key Laboratory of CNC Equipment Reliability, Ministry of Education, School of Mechanical and Aerospace Engineering, Jilin University, Changchun, Jilin 130022, China
[b] Ministry of Education Key Laboratory for Cross-Scale Micro and Nano Manufacturing, Changchun University of Science and Technology, Changchun 130022, China
[c] Key Laboratory of Optical System Advanced Manufacturing Technology, Changchun Institute of Optics, Fine Mechanics and Physics, Chinese Academy of Sciences, Changchun, China

ARTICLE INFO

Keywords:
Micro/nano-structure
Metallic glass
Nanosecond pulsed laser
Ripple
Vein-like structure
Hydrophilicity

ABSTRACT

Formation of regular micro/nano-structures on the surface of metallic glasses (MGs) is beneficial to their functional applications. To pattern the MG surface, in this work, a polished Zr-based MG sample was processed by using a nanosecond pulsed laser under various parameters. Experimental results showed that the regular leaf-shaped microstructure consisting of ripples and vein-like structures was generated in the irradiated area. The effects of processing parameters, including the average power, scanning speed, repetition frequency and pulse overlap rate, on the formation and evolution of leaf-shaped microstructure were investigated in detail. Furthermore, by analyzing the surface characteristics and morphological evolution, the formation mechanism of the leaf-shaped microstructure was analyzed. The ripples with spacing slightly smaller than the wavelength of incident laser were caused by interaction of the incident laser and excited molten surface waves, and the vein-like structures were formed by the subsequent laser pulses induced evolution of precedingly generated micro-cracks. The interaction between the ripples and the vein-like structures resulted in the formation of the leaf-shaped microstructure. After patterning, the MG surface with leaf-shaped microstructure showed enhanced hydrophilicity.

1. Introduction

As a typical amorphous material, metallic glasses (MGs) are free of grain boundary and dislocation compared to traditional metals and crystalline alloys [1,2]. These unique structures endow MGs a series of extraordinary and fascinating properties, such as high strength and elasticity, superior wear and corrosion resistance [3–5]. Therefore, MGs are considered as ideal structural and functional materials [6–11]. On the other hand, fabrication of some regular micro/nano-structures on MGs' surface will significantly enhance their functional applications, such as promoting the cytocompatibility [12], surface coloration [13,14], and tuning the surface wettability [15]. Accordingly, to achieve surface patterning, many methods have been developed to process MGs. For example, by fast tool servo (FTS) assisted diamond turning, Zhu et al. [16] introduced a sinusoidal grid surface on a Zr-based MG, which exhibited high profile accuracy. Via thermoplastic forming, the hole arrays and grating arrays were formed on a Pd-based MG surface, which promoted the application of MGs as mold materials [17]. By chemical etching, randomly distributed nano-pores were generated on a Fe-based MG surface, resulting in the improvement in both hydrophilicity and magnetic properties [18]. Although these processing methods have been proved to be effective for micro/nano-processing of some MGs, they still have some limitations and disadvantages. In general, MGs have relatively high hardness and poor thermal conductivity, so tool wear [19] and potential crystallization and oxidation would occur during mechanical machining [20,21]. For thermoplastic forming, fabrication of molds with micro/nano-structures on them is time-consuming and expensive, and furthermore, the reuse of molds is still difficult due to the difficulty in demolding. With regard to the chemical method, environmental pollution is challenging for large-area patterning of MGs, and also it may be only applicable for some specific MGs. Therefore, exploring new surface patterning methods of MGs is required and meaningful.

Taking advantages of high heating and cooling rates, relatively low

* Corresponding author.
E-mail address: huanghu@jlu.edu.cn (H. Huang).

https://doi.org/10.1016/j.jmapro.2021.10.016
Received 30 June 2021; Received in revised form 22 August 2021; Accepted 8 October 2021
Available online 20 October 2021

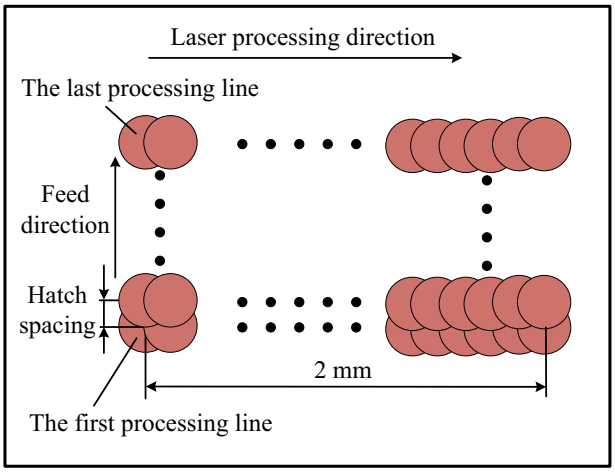

Fig. 1. The schematic diagram illustrating the scanning path during multi-line laser processing.

cost, high efficiency, controllable localized ablation, and environmental friendliness, nanosecond pulsed laser irradiation has been widely employed to fabricate micro/nano-structures on the material surface [22–25]. It has been reported that various micro/nano-structures, such as the porous structure [26], micro-groove [15,27], micro-convex [28] and ripples [29–31], could be generated on the surface of MGs by nanosecond pulsed laser irradiation. Among them, highly-ordered ripples have attracted considerable attention due to their underlying formation mechanism and potential applications [32,33]. However, previous studies mainly focused on the characteristics of localized ripples formed on MG surface after single/multi-pulse nanosecond laser irradiation [29–31]. For practical engineering applications of MGs, the formation of large-area regular ripples is required. Being similar to single/multi-pulse laser irradiation, large-area regular ripples could be generated on the MG surface by nanosecond pulsed laser line processing with appropriate processing parameters. Additionally, micro-cracks are commonly observed in laser processing of MGs [34–36]. It is worth noting that the micro-cracks as a kind of surface defect have some special features such as the enhanced laser absorption compared with the surrounding area [34,37] and affecting the orientation of ripples [38–41]. These features would greatly affect the localized characteristics around the micro-cracks, and the coupling roles of localized ripples and micro-cracks may induce the formation of some unique micro/nano-structures on the MG surface. Accordingly, surface patterning of Zr-based MG was attempted by nanosecond pulsed laser line processing under various experimental parameters. A special leaf-shaped microstructure consisting of ripples and vein-like structures was generated on the MG surface, and the effects of laser parameters on its formation as well as its formation mechanism were further investigated.

2. Experiments

The used MG sample is a typical Zr-based MG ($Zr_{41.2}Ti_{13.8}Cu_{12.5}Ni_{10}Be_{22.5}$). The rod-shaped sample was machined into pieces with thickness of 2 mm by wire-electrical discharge machining (Wire-EDM). As the EDMed surfaces were rough and contained crystallization layers [42,43], these pieces were ground using 400, 800, 1200, 2000 and 3000 grit SiC papers, and then mechanically polished by using a precision lapping/polishing machine (UNIPOL-802, Hefei Kejing Materials Technology Co., LTD, China). After that, the samples were cleaned with acetone and dried in air.

A fiber nanosecond pulsed laser (SP-050P-A-EP-Z-F-Y, SPI Lasers, UK) with a wavelength of 1064 nm and pulse duration of 7 ns was utilized to process the MG samples. The laser beam had a Gaussian energy distribution, and it was focused by using the F-theta lens with a focal length of 160 mm, forming a spot with diameter of ~43 μm on the sample surface. Both single-line and multi-line processing were performed in air. Fig. 1 presents the schematic diagram illustrating the scanning path during multi-line processing. The MG samples were irradiated from the left side to the right side along every line, and the irradiation length was 2 mm. After one-line processing, the laser beam moved a hatch spacing along the feed direction, and then continued the subsequent line irradiation until the set area was completely irradiated. For comparative analysis, various average powers (0.75, 1.0, and 1.5 W), scanning speeds (0.5, 1, and 5 mm/s), repetition frequencies (200, 600, and 1000 kHz), and pulse overlap rates between two adjacent processing lines (28% and 50%) were employed. The processing parameters mentioned above are summarized in Table 1.

Table 1
Laser processing parameters.

Parameter	Value	Unit
Laser wavelength	1064	nm
Laser pulse duration	7	ns
Laser average power	0.75, 1.0, 1.5	W
Laser scanning speed	0.5, 1, 5	mm/s
Repetition frequency	200, 600, 1000	kHz
Pulse overlap rate between two adjacent processing lines	28, 50	%

After laser processing, surface morphologies of the MG were observed by the optical microscope (OM, DSX500, Olympus, Japan), scanning electron microscope (SEM, EVO MA25, ZEISS, Germany), and laser scanning confocal microscope (LSCM, OLS4100, Olympus, Japan). An energy dispersive X-ray spectroscopy (EDS, X-Max20, Oxford Instrument, UK) was utilized to measure the element distribution of the irradiated area. In addition, an optical surface analyser (OSA60, LAUDA Scientific, Germany) was used to measure the contact angles of the originally polished and laser processed surfaces.

3. Results and discussion

3.1. Leaf-shaped microstructure

Fig. 2 shows the typical surface characteristics of the single-line irradiated area. The used average power, scanning speed, and repetition frequency are 1.0 W, 1 mm/s, and 600 kHz, respectively. From the optical image as shown in Fig. 2(a), remarkable heat affected zone (HAZ) is generated on both sides of the processing line; however, it is difficult to clearly distinguish the detailed microstructures in the irradiated area. By SEM observation with higher magnification, the fine microstructures are clearly presented in Figs. 2(b) to (f). Fig. 2(b) presents the surface morphology near the center of the processing line, and Figs. 2(c) and (d) show the surface morphologies around the end point and starting point, respectively. In Fig. 2(b), regular surface microstructure is observed, and it is mainly composed of two kinds of structures, the ripples and the vein-like structures being similar to the veins of the leaf, as shown in the local enlarged view in Fig. 2(f). Furthermore, these two kinds of structures are interlaced with each other, forming the regular leaf-shaped microstructure as shown in Fig. 2(b). From Fig. 2(f), the spacing of the ripples is measured to be about 1 μm, which is approximately equal to the wavelength of the incident laser (1064 nm). Fig. 2(e) gives a local enlarged view of the ripples formed around the starting point. Compared with the ripples formed away from the starting point, the ripples formed around the starting point are small in size and irregular in shape. This indicates that the formation of regular ripples requires continuous action of subsequent laser pulses. Fig. 2(g) shows the three-dimensional (3D) topography of the leaf-shaped microstructure, and Fig. 2(h) shows the cross-sectional profile of the marked line in Fig. 2(g). In the laser irradiated area, the profile is full of ups and downs, and the vein-like structures are low-lying compared to the region between two vein-like structures. The above results demonstrate that the

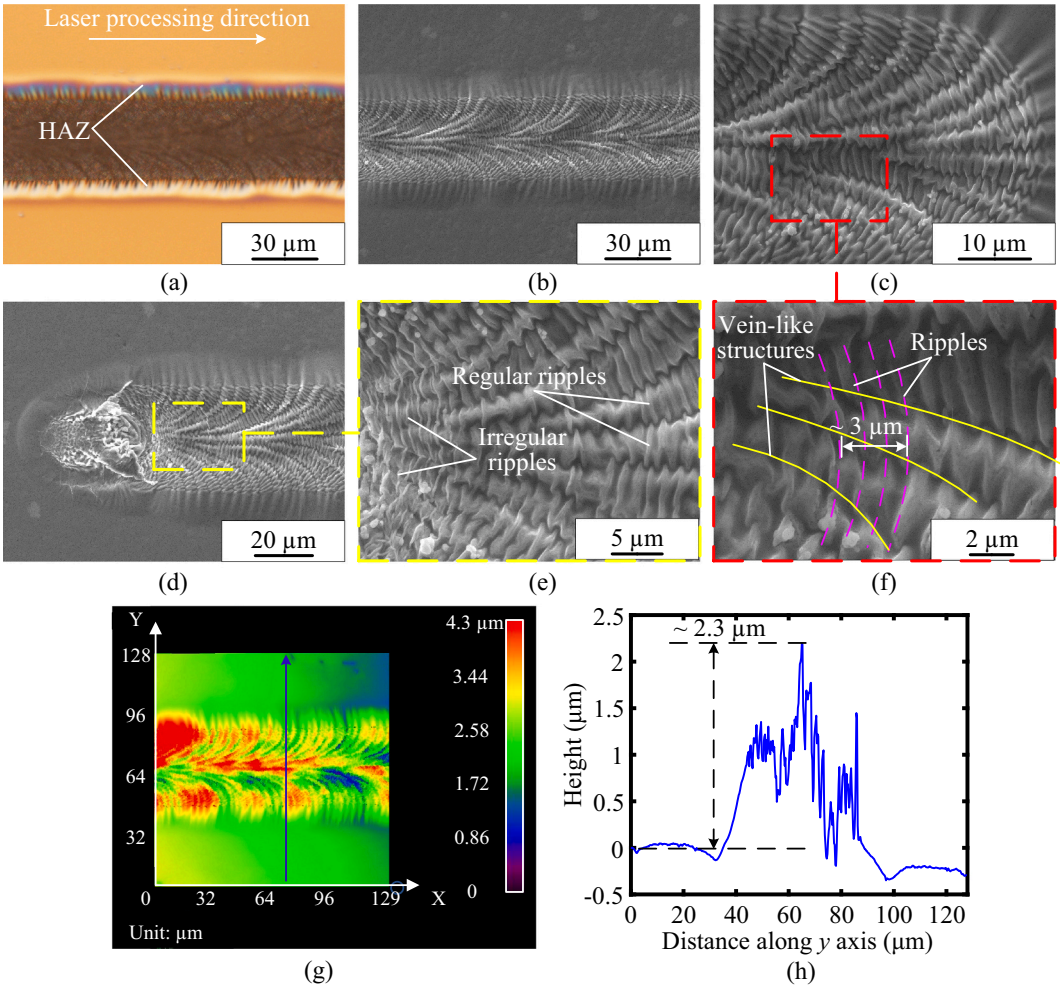

Fig. 2. Surface characteristics of the single-line irradiated area obtained under an average power of 1.0 W, scanning speed of 1 mm/s, and repetition frequency of 600 kHz. (a) Optical image and (b) SEM image near the center area of the processing line. (c) and (d) SEM images around the end point and starting point respectively. (e) and (f) Local enlarged views of Figs. 2(d) and 2(c) respectively, showing the ripples and the vein-like structures in detail. (g) 3D topography of the leaf-shaped microstructure, and (h) the cross-sectional profile of the marked line in Fig. 2(g).

regular leaf-shaped microstructure consisting of ripples and vein-like structures could be formed on the MG surface by nanosecond pulsed laser line processing.

3.2. *Effects of the processing parameters*

In general, several processing parameters such as the average power, scanning speed, repetition frequency, and pulse overlap rate, would affect the laser-material interaction and thus affect the final surface characteristics. Therefore, the effects of these processing parameters on the formation and evolution of leaf-shaped microstructure were further investigated by a series of contrast experiments.

Fig. 3 presents the SEM images of the single-line irradiated areas obtained under the average powers of 1.5 W (Figs. 3(a) and (b)) and 0.75 W (Figs. 3(c) and (d)). Other processing parameters were identical to those in Fig. 2. In Figs. 3(a) and (b), when increasing the average power to 1.5 W, although the entire irradiated area becomes irregular compared to Fig. 2, the ripples and vein-like structures are still generated and furthermore their size increases. In addition, some recast particles with larger size are observed in the irradiated area. In Figs. 3(c) and (d), when the average power decreases to 0.75 W, the ripples being similar to those in Fig. 2 are observed, but the number and size of vein-like structures are significantly reduced compared with those in Figs. 2 and 3(a). Besides, regardless of the increase or decrease in average power, the spacing of the ripples is still about 1 μm. The comparative results in Figs. 3 and 2 indicate that when slightly changing the average power, the size of ripples and vein-like structures will be changed, leading to the change in surface morphology of the leaf-shaped microstructure.

Fig. 4 presents the SEM images of the single-line irradiated areas obtained under the scanning speeds of 0.5 mm/s (Figs. 4(a) and (b)) and 5 mm/s (Figs. 4(c) and (d)). Other processing parameters were identical to those in Fig. 2. As shown in Figs. 4(a) and (b), when decreasing the scanning speed from 1 mm/s to 0.5 mm/s, the leaf-shaped microstructure being similar to that in Fig. 2 is still formed on the MG surface, and the ripple spacing is also about 1 μm. However, when increasing the scanning speed from 1 mm/s to 5 mm/s, very disorganized surface microstructure is observed in the center area; furthermore, the ripples and vein-like structures are very difficult to distinguish. The above results show that the scanning speed has a great influence on the regularity of the surface microstructure.

Fig. 5 presents the SEM images of the single-line irradiated areas obtained under the repetition frequencies of 1000 kHz (Figs. 5(a) and (b)) and 200 kHz (Figs. 5(c) and (d)). Other processing parameters were identical to those in Fig. 2. It is observed that regular leaf-shaped microstructure is still formed when increasing the repetition frequency to 1000 kHz. However, when decreasing the repetition frequency to 200 kHz, the morphology of the whole irradiated area is quite different from

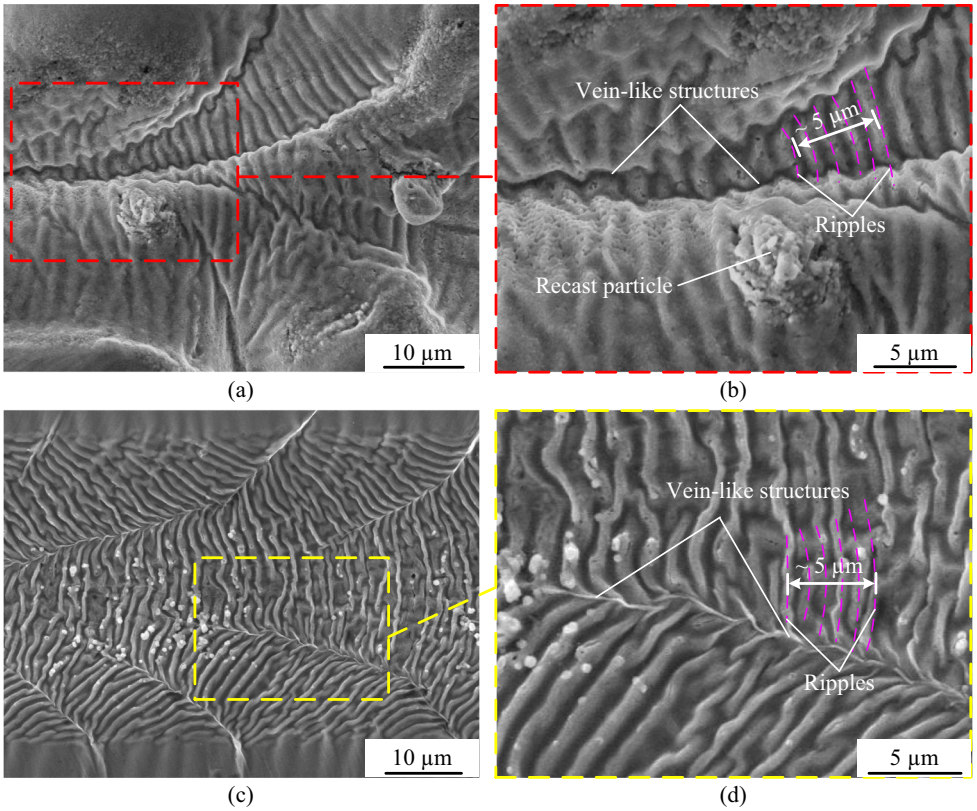

Fig. 3. SEM images of the single-line irradiated areas obtained under different average powers: (a) and (b) 1.5 W; (c) and (d) 0.75 W. Other processing parameters were identical to those in Fig. 2, i.e., scanning speed of 1 mm/s and repetition frequency of 600 kHz.

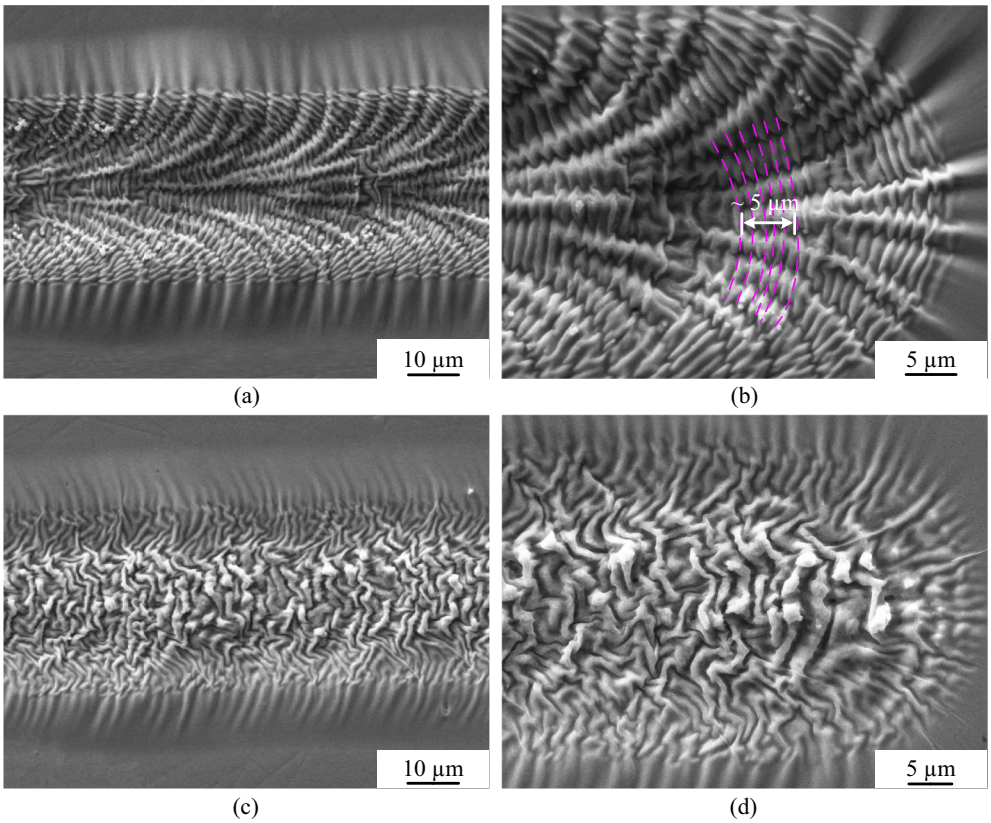

Fig. 4. SEM images of the single-line irradiated areas obtained under different scanning speeds: (a) and (b) 0.5 mm/s; (c) and (d) 5 mm/s. Other processing parameters were identical to those in Fig. 2, i.e., average power of 1.0 W and repetition frequency of 600 kHz.

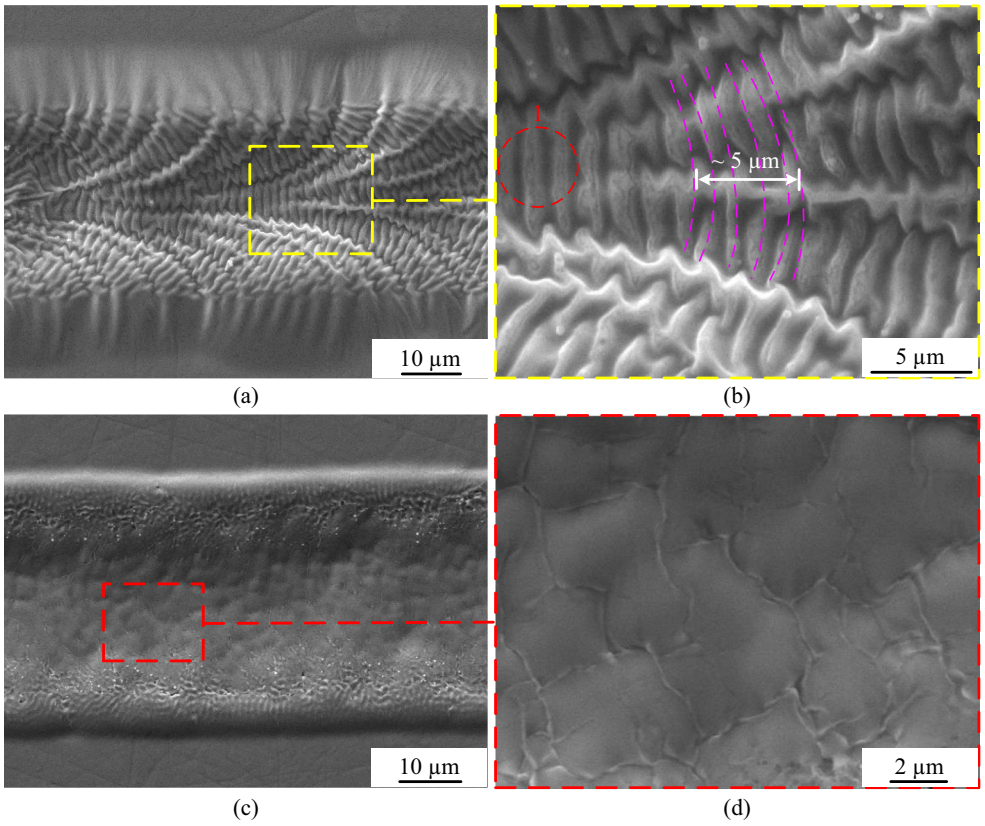

Fig. 5. SEM images of the single-line irradiated areas obtained under different repetition frequencies: (a) and (b) 1000 kHz; (c) and (d) 200 kHz. Other processing parameters were identical to those in Fig. 2, i.e., average power of 1.0 W and scanning speed of 1 mm/s.

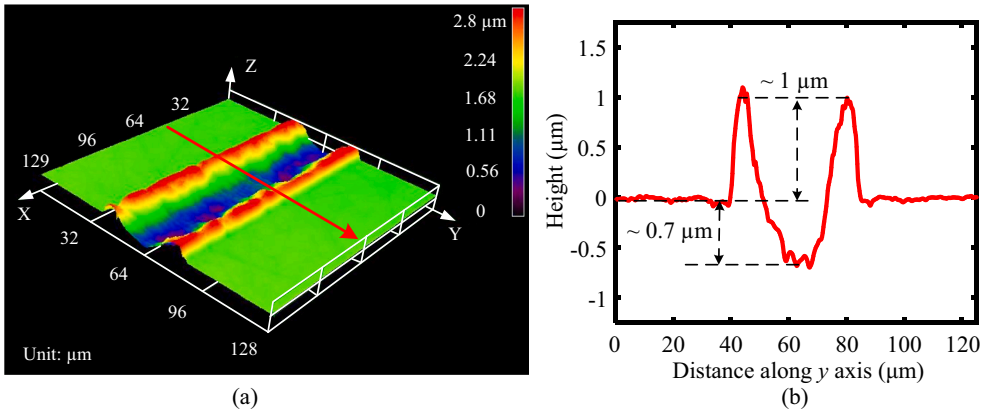

Fig. 6. (a) 3D topography of the single-line irradiated area obtained under the repetition frequency of 200 kHz, and (b) the cross-sectional profile along the marked line in Fig. 6(a). Other processing parameters were identical to those in Fig. 5, i.e., average power of 1.0 W and scanning speed of 1 mm/s.

those obtained under other processing parameters. As shown in Fig. 5 (d), a smooth irradiated area with neither ripples nor vein-like structures was observed. Fig. 6(a) shows the 3D topography of the irradiated area obtained under the repetition frequency of 200 kHz, and Fig. 6(b) presents the cross-sectional profile of the marked line in Fig. 6(a). Instead of the leaf-shaped microstructure, the micro-groove structure is generated on the MG surface when decreasing the repetition frequency to 200 kHz. The difference in surface morphology under various repetition frequencies could be due to the huge difference in single-pulse energy (E), which can be expressed as

$$E = \frac{P_{avg}}{f} \quad (1)$$

where P_{avg} is the average power and f is the repetition frequency. Accordingly, when keeping the average power unchanged, the single-pulse energy at 200 kHz is three times of that at 600 kHz. Therefore, at 200 kHz, more MG materials would be molten and pushed to both sides of the processing line with the role of recoil pressure, leading to the transition from the leaf-shaped microstructure to the micro-groove structure.

Fig. 7 presents the SEM images of the multi-line irradiated areas obtained under two different pulse overlap rates r, 28% (Figs. 7(a) and (b)) and 50% (Figs. 7(c) and (d)). Other processing parameters were identical to those in Fig. 2. In Figs. 7(a) and (b), when the pulse overlap rate r is 28%, the surface morphology of each processing line is very

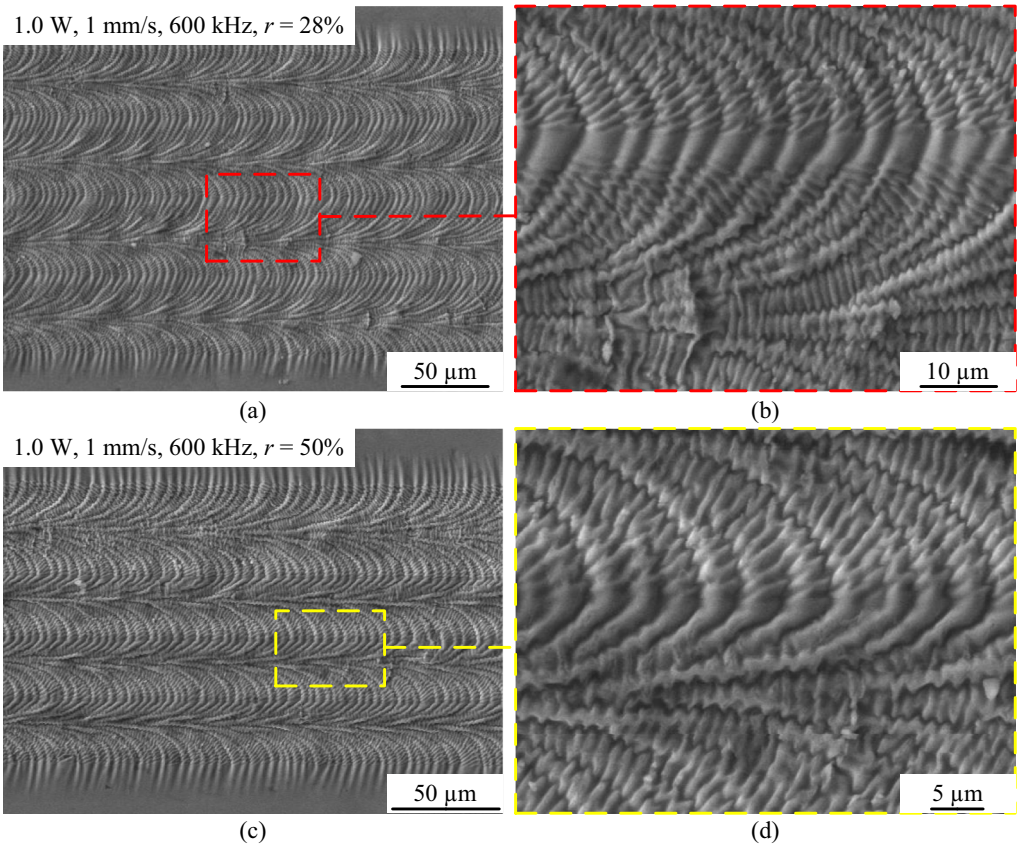

Fig. 7. SEM images of the multi-line irradiated areas obtained under different pulse overlap rates: (a) and (b) 28%; (c) and (d) 50%. Other processing parameters were identical to those in Fig. 2, i.e., average power of 1.0 W, scanning speed of 1 mm/s, and repetition frequency of 600 kHz.

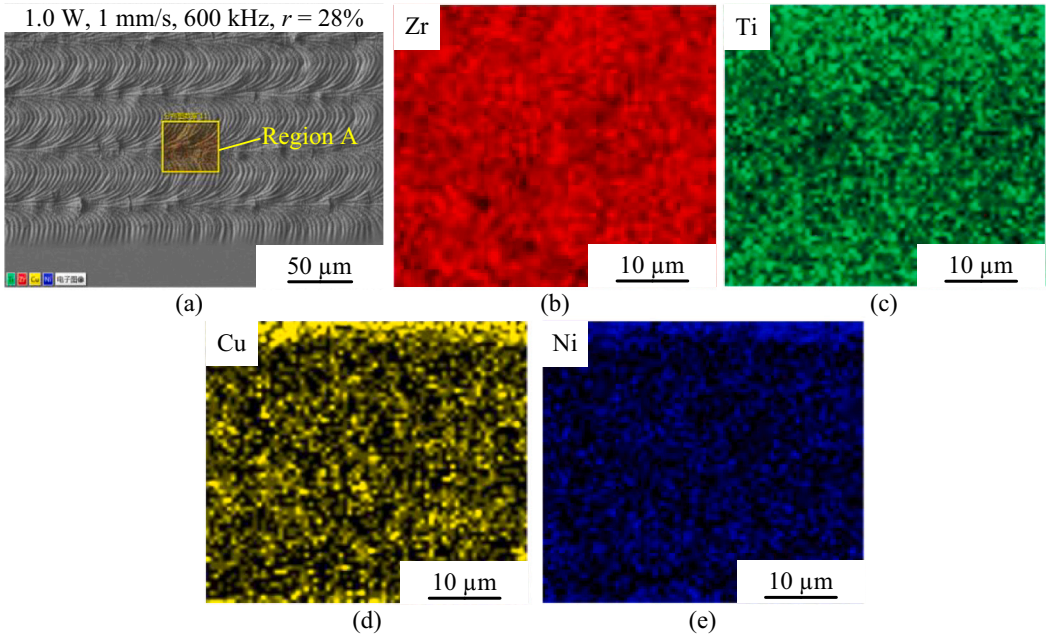

Fig. 8. (a) EDS testing region, Region A, and (b)–(e) show the element distribution of (b) Zr, (c) Ti, (d) Cu, and (e) Ni.

similar to that after single-line processing as shown in Fig. 2(b), and two adjacent processing lines are well connected in the HAZ of each processing line. When shifting the pulse overlap rate from 28% to 50%, the connection position of two adjacent processing lines moves from the HAZ to near the center of the preceding processing line. The results in Fig. 7 indicate that regular large-area leaf-shaped microstructure can be fabricated on the MG surface by multi-line processing, and the connection position of adjacent processing lines can be controlled by changing the pulse overlap rate.

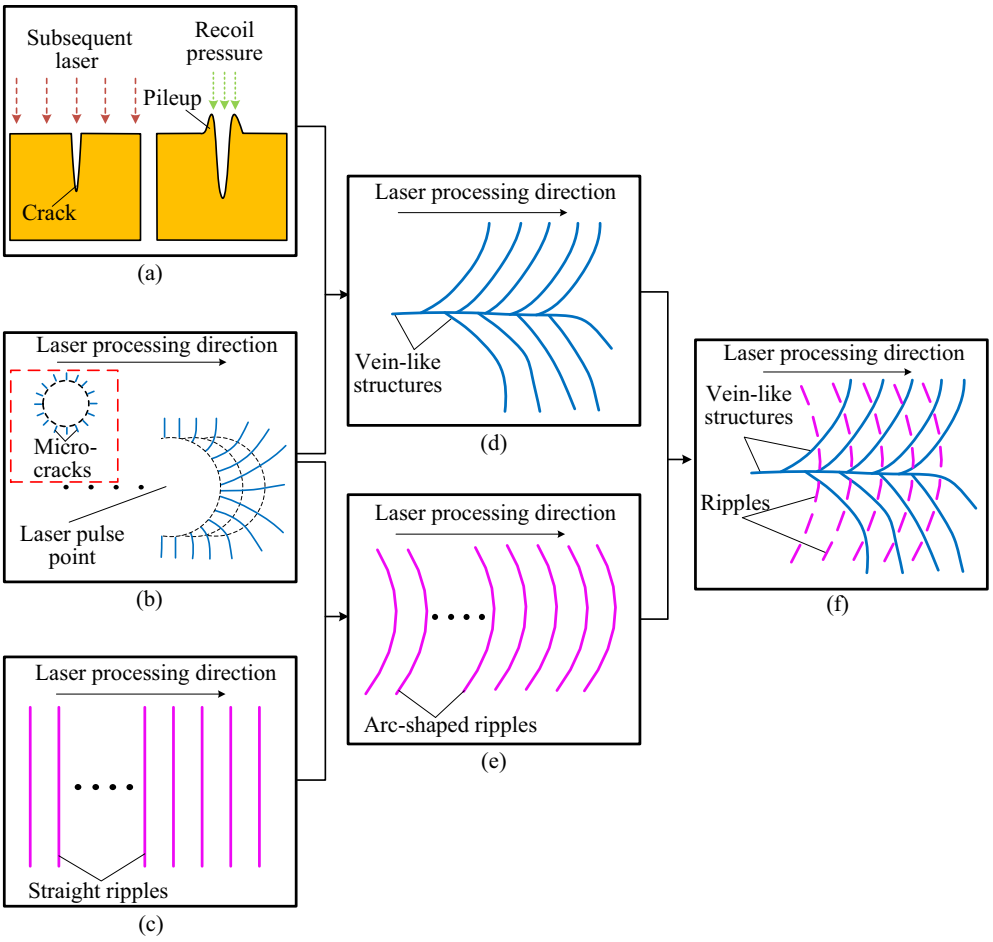

Fig. 9. Schematic diagram illustrating the formation of leaf-shaped microstructure. (a) Schematic diagram showing the formation of pileup around the micro-cracks, (b) schematic diagram showing the moving of laser pulse and the evolution of micro-cracks (the inserted figure illustrating the morphology after multi-pulse laser irradiation), (c) formation of the straight ripples, (d) formation of the vein-like structures, (e) formation of arc-shaped ripples with the influence of micro-cracks, and (f) intersection of the vein-like structures and ripples.

3.3. *Formation mechanism of the leaf-shaped microstructure*

To better tune the leaf-shaped microstructure, understanding its formation mechanism is the premise and foundation. In some cases, the micro/nano-structures formed by laser processing are accompanied by the enrichment of elements [34]. Therefore, the distribution of elements in the laser irradiated area was first measured by EDS. Fig. 8(a) shows the testing region, Region A, which is located in the multi-line irradiated area. Figs. 8(b)–(e) present the mapping results of elements Zr, Ti, Cu, and Ni, respectively. Be element is not detected owing to its small atomic mass. From Fig. 8, it is noted that all elements are uniformly distributed in the measured Region A, demonstrating that no element enrichment occurs during laser processing of MG under the employed experimental parameters.

According to Fig. 8, the formation of leaf-shaped microstructure does not originate from element enrichment. As the leaf-shaped microstructure is composed of two kinds of detailed structures, the ripples and the vein-like structures, their formation mechanisms will be discussed separately.

For ripples, it is a universal phenomenon induced by laser-material

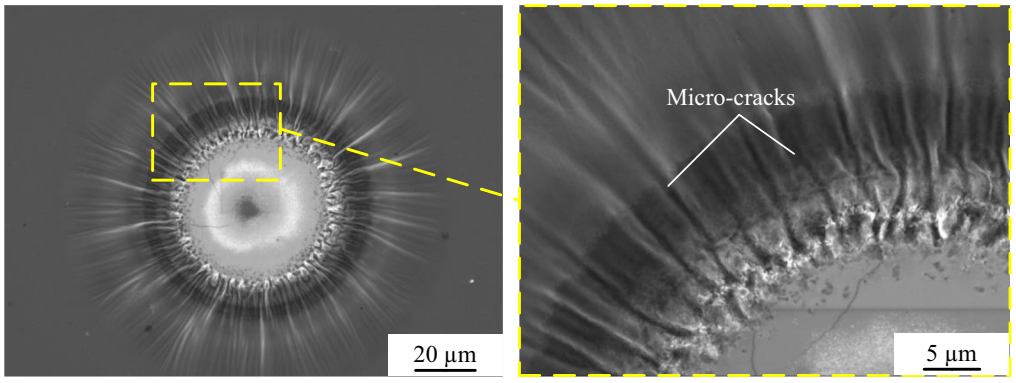

Fig. 10. (a) SEM image of the laser irradiated areas obtained under an average power of 1 W, number of laser pulses of 1200, and repetition frequency of 600 kHz. (b) Local enlarged view of Fig. 10(a).

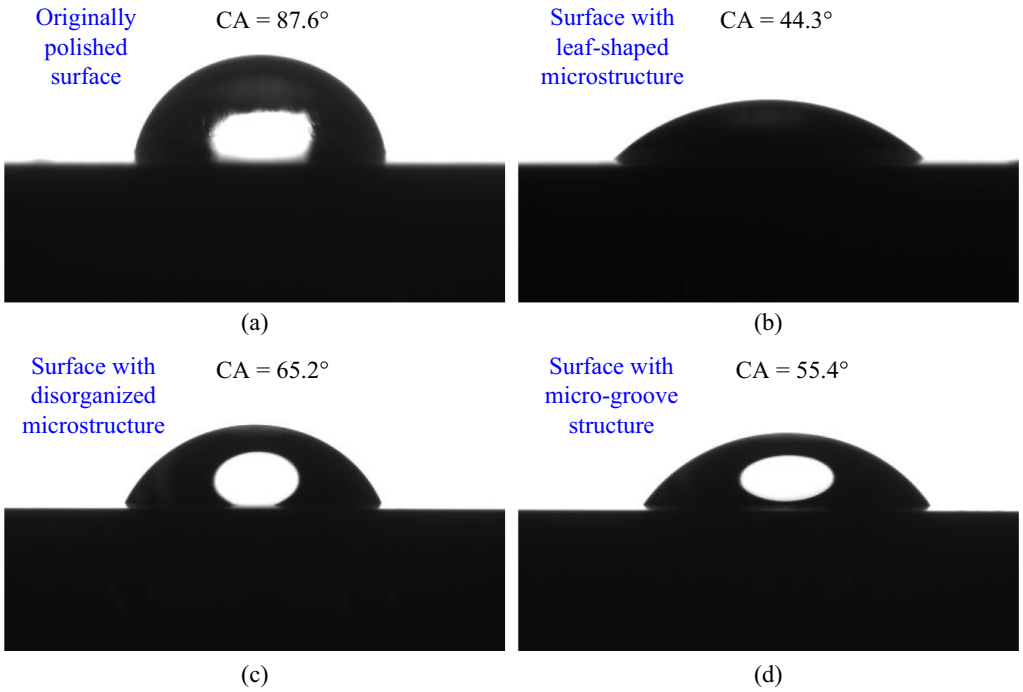

Fig. 11. Droplets shapes on the surfaces of Zr-based MGs: (a) originally polished surface, (b) surface with leaf-shaped microstructure, (c) surface with disorganized microstructure, and (d) surface with micro-groove structure.

interaction, and their spacing is directly determined by the corresponding formation mechanism [30,33]. In this paper, the spacing of ripples does not change with the scanning speed and repetition frequency, demonstrating that these ripples are not the typical laser pulse tracks [34]. Furthermore, as shown in Fig. 2(d), the ripples only appear on the right side of the starting point and not on the left side. This is obviously different from the concentric circular ripples formed by single/multi-pulse ablation of MGs, so the corresponding hydrodynamic mechanism should also be excluded [29,30]. It is worth noting that the spacing of ripples is always slightly smaller than the wavelength of the incident laser (1064 nm), which is very consistent with the periodic characteristics of classical low spatial frequency laser induced periodic surface structures (LSFL). Therefore, it can be inferred that ripples are actually the classical LSFL. Generally, the analysis of the formation mechanism of classical LSFL needs to refer to the thermal history of its formation. By comparing the 3D topographies of Figs. 2(g) and 6(a), it can be concluded that when decreasing the repetition frequency from 600 kHz to 200 kHz, the surface microstructure will transform from the slightly convex leaf-shaped microstructure to the typical inverted Gaussian-shaped micro-groove structure. This means that when laser irradiation is performed using the processing parameters in Fig. 2, the deposited laser energy is insufficient to cause surface ablation, and the MG surface only experiences melting and rapid solidification. Accordingly, the interaction of the incident laser and excited molten surface waves may dominate the formation of this low spatial frequency ripples [33]. In this case, the deposited optical energy is not enough to remove the material, but the rapid solidification of the molten area will lead to the change in surface topography, resulting in periodic ripples.

For vein-like structures, their formation may originate from the evolution of micro-cracks during the laser line processing. Figs. 9(a), (b) and (d) illustrate the possible formation mechanism of vein-like structures. In some previous studies [35], it is widely reported that after single pulse laser irradiation, the micro-crater will be generated on the Zr-based MG surface, and around the micro-crater, some micro-cracks are uniformly distributed. This could be further confirmed by the SEM images shown in Figs. 10(a) and (b), which are obtained by multi-pulse laser irradiation under an average power of 1 W, number of laser pulses of 1200, and repetition frequency of 600 kHz. During the laser line processing, as the distance between two adjacent laser pulses is very small (especially the repetition frequency used in this study is quite high), the micro-cracks formed in preceding pulse irradiation are still in the affected zone of some subsequent pulses. Compared with the non-cracking regions, the cracking regions have stronger capacity to absorb the energy of the subsequent laser pulses [37]. Therefore, as shown in Fig. 9(a), localized re-melting would readily occur around the micro-cracks during the following laser line processing, and then the temperature around the micro-cracks would rise sharply, even exceeding the vaporization temperature. With the role of recoil pressure, the molten materials at the micro-cracks would flow outward, forming the pileup. This process is very similar to the process when single pulse laser is irradiated on the MG surface, resulting in the formation of the micro-crater with pileup around it. As the laser pulse moves along one line, the cracking regions will connect together, forming the vein-like structures as illustrated in Fig. 9(d). At the same time, the generated pileups between two micro-cracks could combine together to form the localized high-lying pileup. This is the reason why the vein-like structures are low-lying compared to the regions between two vein-like structures.

In general, the laser-induced ripples are perpendicular or parallel to the polarization direction of the laser. However, the ripples generated in this paper are arc-shaped. Figs. 9(b), (c) and (e) illustrate the possible reason. Being similar to those surface scratches and debris, micro-cracks as a kind of surface defect also have a significant influence on the orientation of ripples [38–41]. Therefore, the orientation of ripples changes greatly near the micro-cracks, while the ripples unaffected by the micro-cracks remain straight as shown in region 1 in Fig. 5(b). Finally, during the laser line processing, the vein-like structures and arc-shaped ripples were interlaced with each other, leading to the formation of regular leaf-shaped microstructure as illustrated in Fig. 9(f).

3.4. Discussion on the effects of processing parameters

According to the formation mechanism illustrated in Fig. 9, the effects of laser processing parameters on the surface microstructure will be

Table 2
The surface roughness of the originally polished and laser processed MG surfaces.

	Originally polished surface	Surface with leaf-shaped microstructure	Surface with disorganized microstructure	Surface with micro-groove structure
Surface roughness (μm)	0.006	1.265	0.437	0.864

further discussed as follows.

As for the effects of average power, with its increase, the laser-induced thermal stress will increase, and therefore the formation of micro-cracks will be promoted. Meanwhile, at a higher average power, localized re-melting around the micro-cracks will be enhanced as well, resulting in the increase in size of pileups around the micro-cracks, and vice versa. Accordingly, the surface morphology of the leaf-shaped microstructure is changed when changing the average power.

As for the effects of scanning speed, when increasing the scanning speed from 1 mm/s to 5 mm/s, the distance between adjacent laser pulses is increased by four times. Therefore, the influence of subsequent laser pulses on the preceding irradiated area will be weakened, and the heat accumulation is reduced as well. These effects not only inhibit the formation of micro-cracks, but also affect the regularity of the ripples, which ultimately lead to the formation of very disorganized surface microstructure as shown in Fig. 4(c). In contrast, when decreasing the scanning speed from 1 mm/s to 0.5 mm/s, the formation of micro-cracks is slightly promoted and the size of ripples is slightly increased, showing slight effect on the surface morphology.

As for the effects of repetition frequency, when increasing the repetition frequency from 600 kHz to 1000 kHz, the single-pulse energy will slightly decrease, resulting in the suppression of micro-cracks and reduction in size of ripples. On the other hand, the increased number of laser pulses per unit length will promote the formation of micro-cracks and also increase the size of ripples. These two effects balance each other, and thus the surface morphology is not significantly changed when increasing the repetition frequency. However, when decreasing the repetition frequency from 600 kHz to 200 kHz, the single-pulse energy is increased by two times. At such high single-pulse energy, the recoil pressure will dominate the flow of melts, leading to the formation of the typical micro-groove structure on the MG surface.

In addition, since the ripples are caused by the interaction of the incident laser and excited molten surface waves, the spacing of ripples remains the same no matter how the laser processing parameters are changed.

3.5. Effects of microstructure on surface wettability

An important application of fabricating microstructures on material surface is to tune the surface wettability [44–47]. For MGs, the known applications for tuning their surface wettability include improved cytocompatibility [12] and directional transport of microdroplets [48]. To investigate the effects of the formed surface microstructures on the surface wettability, the contact angles (CAs) of the laser processed MG surfaces with different surface microstructures (including the leaf-shaped microstructure as shown in Fig. 2, the disorganized microstructure as shown in Figs. 4(c) and (d), and the micro-groove structure as shown in Figs. 5(c) and (d)) were measured. For comparison, the CA of the originally polished surface was also measured. During the experiments, deionized water with volume of 5 μl was employed to contact the surface. The CA of polished surface is 87.6° as shown in Fig. 11(a), demonstrating its intrinsic hydrophilicity. In contrast, the CAs of all laser processed surfaces are reduced, as evidenced by the obtained CAs shown in Figs. 11(b) to (d). Among them, the MG surface with leaf-shaped microstructure shows more significant hydrophilicity, with the CA of 44.3°. The decrease in CA may be caused by the change in surface roughness after laser processing. To verify this, the surface roughness of the originally polished and laser processed surfaces were tested, and the corresponding results are presented in Table 2. The results indicate that the surface roughness of the laser processed surface is significantly higher than that of the originally polished surface. In addition, the surface with leaf-shaped microstructures has the largest surface roughness (1.265 μm). Previous studies [15,47,49] have reported that surface roughness plays a crucial role in wettability. When the original surface is hydrophobic, the increased surface roughness will make it more hydrophobic; while the hydrophilic surface will become more hydrophilic with the increase of surface roughness [15,50]. Compared to the originally polished surface, the roughness of the processed surface is increased, resulting in the decrease in CA, i.e., enhanced hydrophilicity. Correspondingly, the smallest CA of the surface with leaf-shaped microstructure is consistent with its largest surface roughness. The increase in hydrophilicity would be meaningful for MGs working as biomaterials because it would improve the cell adhesion.

4. Conclusions

In summary, by nanosecond pulsed laser irradiation in air, a regular leaf-shaped microstructure was generated on a Zr-based MG surface, and it mainly consisted of two kinds of structures, the ripples and the vein-like structures. Comparative experiments indicated that the formation of regular leaf-shaped microstructure greatly depended on the applied laser processing parameters. The change in average power would change the size of ripples and vein-like structures, and thus affect the surface morphology of the leaf-shaped microstructure. The increase in scanning speed from 1 to 5 mm/s would lead to disorder of the surface microstructure. When processing with a relatively low repetition frequency (200 kHz), the typical micro-groove structure was formed instead of the leaf-shaped microstructure. By multi-line laser processing, the large-area leaf-shaped microstructure could be generated, and the connection position between two adjacent processing lines was controlled by the pulse overlap rate. By analyzing the surface characteristics and morphological evolution, formation mechanisms of the ripples and the vein-like structures were discussed, and their interaction during the laser line processing resulted in the final leaf-shaped microstructure. Compared with the originally polished surface, the laser processed MG surfaces exhibited enhanced hydrophilicity, which would be meaningful for MGs working as functional materials.

Data availability

The raw/processed data required to reproduce these findings cannot be shared at the time of submission due to technical or time limitations.

Declaration of competing interest

The authors declare that they have no known competing financial interests or personal relationships that could have appeared to influence the work reported in this paper.

Acknowledgements

This work was supported by the National Natural Science Foundation of China (Grant No. 51705197), the Young Elite Scientists Sponsorship Program by CAST (YESS) (Grant No. 2017QNRC001), the Graduate Innovation Fund of Jilin University (Grant No. 101832020CX106), and the Fundamental Research Funds for the Central Universities (2019-

2021).

References

[1] Yavari AR, Lewandowski JJ, Eckert J. Mechanical properties of bulk metallic glasses. MRS Bull 2007;32:635–8.
[2] Schuh CA, Hufnagel TC, Ramamurty U. Mechanical behavior of amorphous alloys. Acta Mater 2007;55:4067–109.
[3] Trexler MM, Thadhani NN. Mechanical properties of bulk metallic glasses. Prog Mater Sci 2010;55:759–839.
[4] Scully JR, Gebert A, Payer JH. Corrosion and related mechanical properties of bulk metallic glasses. J Mater Res 2007;22:302–13.
[5] Plummer J, Johnson WL. Is metallic glass poised to come of age? Nat Mater 2015; 14:553–5.
[6] Jafary-Zadeh M, Kumar GP, Branicio PS, Seifi M, Lewandowski JJ, Cui FS. A critical review on metallic glasses as structural materials for cardiovascular stent applications. J Funct Biomater 2018;9:19.
[7] Ashby MF, Greer AL. Metallic glasses as structural materials. Scr Mater 2006;54: 321–6.
[8] Inoue A, Nishiyama N. New bulk metallic glasses for applications as magnetic-sensing, chemical, and structural materials. MRS Bull 2007;32:651–8.
[9] Li N, Xia T, Heng LP, Liu L. Superhydrophobic Zr-based metallic glass surface with high adhesive force. Appl Phys Lett 2013;102:251603.
[10] Schroers J, Nguyen T, O'Keeffe S, Desai A. Thermoplastic forming of bulk metallic glass—applications for MEMS and microstructure fabrication. Mater Sci Eng A 2007;449–51:898–902.
[11] Liu X, Shao Y, Lu S-Y, Yao K-F. High-accuracy bulk metallic glass mold insert for hot embossing of complex polymer optical devices. J Polym Sci Pol Physics 2015; 53:463–7.
[12] Jiao Y, Brousseau E, Ayre WN, Gait-Carr E, Shen XJ, Wang XX, et al. In vitro cytocompatibility of a Zr-based metallic glass modified by laser surface texturing for potential implant applications. Appl Surf Sci 2021;547:149194.
[13] Gao Q, Ouyang D, Liu XT, Wu SX, Huang X, Li N. Fabricating colorful bulk metallic glass surfaces by femtosecond laser processing. Mater Chem Phys 2021;266: 124561.
[14] Zhang HY, Qian YF, Zhang L, Zhang D, Liu HL, Huang H. Surface coloration of Zr-based metallic glass by nanosecond pulsed laser irradiation in ambient atmosphere. Mater Lett 2021;304:130721.
[15] Jiao Y, Brousseau E, Shen XJ, Wang XX, Han QQ, Zhu HX, et al. Investigations in the fabrication of surface patterns for wettability modification on a Zr-based bulk metallic glass by nanosecond laser surface texturing. J Mater Process Technol 2020;283:116714.
[16] Zhu ZW, Zhou XQ, Liu Q, Lin JQ, Zhao SX. Fabrication of micro-structured surfaces on bulk metallic glasses based on fast tool servo assisted diamond turning. Sci Adv Mater 2012;4:906–11.
[17] Yang C, L-m Lu, Z-w Zhao, J-h Li, Gong F, Ma J. Micro thermoplastic forming of a Pd-based metallic glass: theory and applications. J Iron Steel Res Int 2017;24: 378–84.
[18] Zhang HY, Fornell J, Feng YP, Golvano I, Baró MD, Pellicer E, et al. Inducing surface nanoporosity on Fe-based metallic glass matrix composites by selective dealloying. Mater Charact 2019;153:46–51.
[19] Bakkal M, Shih AJ, Scattergood RO. Chip formation, cutting forces, and tool wear in turning of Zr-based bulk metallic glass. Int J Mach Tool Manu 2004;44:915–25.
[20] Bakkal M, Liu CT, Watkins TR, Scattergood RO, Shih AJ. Oxidation and crystallization of Zr-based bulk metallic glass due to machining. Intermetallics 2004;12:195–204.
[21] Bakkal M, Shih AJ, Scattergood RO, Liu CT. Machining of a Zr–Ti–Al–Cu–Ni metallic glass. Scr Mater 2004;50:583–8.
[22] Wang C, Huang H, Qian YF, Zhang ZY, Yan JW. One-step fabrication of regular hierarchical micro/nano-structures on glassy carbon by nanosecond pulsed laser irradiation. J Manuf Process 2021;62:108–18.
[23] Wang QH, Samanta A, Toor F, Shaw S, Ding HT. Colorizing Ti-6Al-4V surface via high-throughput laser surface nanostructuring. J Manuf Process 2019;43:70–5.
[24] Samanta A, Wang QH, Singh G, Shaw SK, Toor F, Ratner A, et al. Nanosecond pulsed laser processing turns engineering metal alloys antireflective and superwicking. J Manuf Process 2020;54:28–37.
[25] Peláez RJ, Rebollar E, Serna R, Acosta-Zepeda C, Saavedra P, Bonse J, et al. Nanosecond laser-induced interference grating formation on silicon. J Phys D 2019;52:225302.
[26] Jiang MQ, Wei YP, Wilde G, Dai LH. Explosive boiling of a metallic glass superheated by nanosecond pulse laser ablation. Appl Phys Lett 2015;106:021904.
[27] Huang H, Jun N, Jiang MQ, Ryoko M, Yan JW. Nanosecond pulsed laser irradiation induced hierarchical micro/nanostructures on Zr-based metallic glass substrate. Mater Des 2016;109:153–61.
[28] Qian YF, Jiang MQ, Zhang ZY, Huang H, Yan JW. On the transformation between micro-concave and micro-convex in nanosecond laser ablation of a Zr-based metallic glass. J Manuf Process 2021;68:1114–22.
[29] Zhu YH, Fu J, Zheng C, Ji Z. Effect of nanosecond pulse laser ablation on the surface morphology of Zr-based metallic glass. Opt Laser Technol 2016;83:21–7.
[30] Liu Y, Jiang MQ, Yang GW, Guan YJ, Dai LH. Surface rippling on bulk metallic glass under nanosecond pulse laser ablation. Appl Phys Lett 2011;99:191902.
[31] Liu WD, Ye LM, Liu KX. Micro-nano scale ripples on metallic glass induced by laser pulse. J Appl Phys 2011;109:043109.
[32] Florian C, Kirner SV, Krüger J, Bonse J. Surface functionalization by laser-induced periodic surface structures. J Laser Appl 2020;32:022063.
[33] Bonse J, Hohm S, Kirner SV, Rosenfeld A, Kruger J. Laser-induced periodic surface structures— a scientific evergreen. IEEE J Sel Top Quant Electron 2017;23:109–23.
[34] Huang H, Yan JW. Surface patterning of Zr-based metallic glass by laser irradiation induced selective thermoplastic extrusion in nitrogen gas. J Micromech Microeng 2017;27:075007.
[35] Huang H, Noguchi J, Yan JW. Shield gas induced cracks during nanosecond-pulsed laser irradiation of Zr-based metallic glass. Appl Phys A Mater Sci Process 2016; 122:881.
[36] Huang H, Qian YF, Wang C, Yan JW. Laser induced micro-cracking of Zr-based metallic glass using 10^{11} W/m^2 nano-pulses. Mater Today Commun 2020;25: 101554.
[37] Feit MD, Rubenchik AM. Influence of subsurface cracks on laser-induced surface damage. SPIE 2004;5273:264–72.
[38] Ardron M, Weston N, Hand D. A practical technique for the generation of highly uniform LIPSS. Appl Surf Sci 2014;313:123–31.
[39] Li C, Cheng G-H, Colombier J-P, Faure N, Reynaud S, Zhang H, et al. Impact of evolving surface nanoscale topologies in femtosecond laser structuring of Ni-based superalloy CMSX-4. J Opt 2016;18:015402.
[40] Preusch F, Rung S, Hellmann R. Influence of polishing orientation on the generation of LIPSS on stainless steel. J Laser Micro/Nanoeng 2016;11:137–42.
[41] Soileau MJ. Ripple structures associated with ordered surface defects in dielectrics. IEEE J Quantum Elect 1984;20:464–7.
[42] Huang H, Yan JW. Microstructural changes of Zr-based metallic glass during micro-electrical discharge machining and grinding by a sintered diamond tool. J Alloys Compd 2016;688:14–21.
[43] Huang H, Yan JW. On the surface characteristics of a Zr-based bulk metallic glass processed by microelectrical discharge machining. Appl Surf Sci 2015;355: 1306–15.
[44] Huerta-Murillo D, García-Girón A, Romano JM, Cardoso JT, Cordovilla F, Walker M, et al. Wettability modification of laser-fabricated hierarchical surface structures in Ti-6Al-4V titanium alloy. Appl Surf Sci 2019;463:838–46.
[45] Long JY, Fan PX, Jiang DF, Han JP, Lin Y, Cai MY, et al. Anisotropic sliding of water droplets on the superhydrophobic surfaces with anisotropic groove-like micro/nano structures. Adv Mater Interfaces 2016;3:1600641.
[46] Ma J, Zhang XY, Wang DP, Zhao DQ, Ding DW, Liu K, et al. Superhydrophobic metallic glass surface with superior mechanical stability and corrosion resistance. Appl Phys Lett 2014;104:173701.
[47] Xia T, Li N, Wu Y, Liu L. Patterned superhydrophobic surface based on Pd-based metallic glass. Appl Phys Lett 2012;101:081601.
[48] Li C, Yang LJ, Ren XZ, Yang Y, Cheng GH. Femtosecond laser-induced non-centrosymmetric surface microstructures on bulk metallic glass for unidirectional droplet micro-displacement. J Phys D 2020;53:105305.
[49] Genzer J, Efimenko K. Creating long-lived superhydrophobic polymer surfaces through mechanically assembled monolayers. Science 2000;290:2130–3.
[50] Wenzel RN. Resistance of solid surfaces to wetting by water. Ind Eng Chem 1936; 28:988–94.